International Journal of Nanomedicine

Dovepress
open access to scientific and medical research

Open Access Full Text Article

ORIGINAL RESEARCH

Gold quantum dots impair the tumorigenic potential of glioma stem-like cells via β-catenin downregulation in vitro

This article was published in the following Dove Medical Press journal:
International Journal of Nanomedicine

Rizwan Wahab[1,2,*]
Neha Kaushik[3,*]
Farheen Khan[4]
Nagendra Kumar Kaushik[5]
Su-Jae Lee[3]
Eun Ha Choi[5]
Abdulaziz A Al-Khedhairy[1]

[1]Zoology Department, College of Science, King Saud University, Riyadh 11451, Saudi Arabia; [2]Al-Jeraisy, Chair for DNA Research, King Saud University, Riyadh 11451, Saudi Arabia; [3]Department of Life Science, Hanyang University, Seoul 04763, South Korea; [4]Chemistry Department, Faculty of Science, Taibah University, Yanbu 42353, Saudi Arabia; [5]Plasma Bioscience Research Center/Applied Plasma Medicine Center, Department of Electrical and Biological Physics, Kwangwoon University, Seoul 01897, South Korea

*These authors contributed equally to this work

Correspondence: Nagendra Kumar Kaushik
Plasma Bioscience Research Center/ Applied Plasma Medicine Center, Department of Electrical and Biological Physics, Kwangwoon University, 20 Gwangun-ro, Wolgye 1(il)-dong, Nowon-gu, Seoul 01897, South Korea
Tel +82 29 40 8618
Fax +82 29 40 5664
Email kaushik.nagendra@kw.ac.kr

Rizwan Wahab
Al-Jeraisy, Chair for DNA Research, Zoology Department, College of Science, King Saud University, PO Box 2455, Riyadh 11451, Saudi Arabia
Tel +966 5 3602 3284
Email rwahab@ksu.edu.sa

Background: Over the past several decades, the incidence of solid cancers has rapidly increased worldwide. Successful removal of tumor-initiating cells within tumors is essential in the field of cancer therapeutics to improve patient disease-free survival rates. The biocompatible multivarient-sized gold nanoparticles (MVS-GNPs) from quantum dots (QDs, <10 nm) to nanosized (up to 50 nm) particles have vast applications in various biomedical areas including cancer treatment. The role of MVS-GNPs for inhibition of tumorigenic potential and stemness of glioma was investigated in this study.

Methods: Herein, MVS-GNPs synthesized and characterized by means of X-ray diffraction pattern (XRD) and transmission electron microscopy (TEM) techniques. Afterwards, interaction of these GNPs with glioma stem-cell like cells along with cancer cells were evaluated by MTT, cell motility, self-renewal assays and biostatistics was also applied.

Results: Among these GNPs, G-QDs contributed to reduce metastatic events and spheroid cell growth, potentially blocking the self-renewal ability of these cells. This study also uncovers the previously unknown role of the inhibition of CTNNB1 signaling as a novel candidate to decrease the tumorigenesis of glioma spheroids and subsequent spheroid growth. The accurate and precise biostatistics results were obtained at quantify level.

Conclusion: In summary, G-QDs may exhibit possible contribution on suppressing the growth of tumor-initiating cells. These data reveal a unique therapeutic approach for the elimination of residual resistant stem-like cells during cancer treatment.

Keywords: multivarient gold nanoparticles, epithelial-mesenchymal transition, solid tumor, brain cancer, self-renewal, cellular movement, biostatistics

Introduction

Gold nanoparticle (GNP) is the most valuable colloidal inorganic material in current research on nanotechnology owing to its various industrial and biomedical applications.[1] In relation to nanotechnology, particle size is an important and interesting parameter that affects the surfaces of particles and forms various types of structures, such as quantum, nano-, micro-, and macrostructures. A zero-dimension material, quantum dots (QDs) exhibit very small dimensions of 2–10 nm, and these molecules have diameters of about 10–50 atoms.[2] Due to their small size, they exhibit larger surface areas of the crystals, the highest valence, and the lowest conduction bands, and they release more energy when the crystals return to their resting state. Another category is the larger dimensions of QDs, which are nanoparticles (NPs) in the range of 1–100 nm, and it is assumed that QDs and NPs are very small in size and shape in nanostructure family. Owing to these advantages, they can enter any type of biological identity/target,

such as cells and microbes.[3] As per the published literature, a small nano-range (~1–100 nm) of GNPs can be obtained via citrate transfer method, with thermal and ion irritation used to reduce gold chloride and produce small GNPs.[4,5] GNPs have numerous biomedical applications in various areas, such as drug delivery in osteoarthritis disease[6] and in others related to hippocampal CA1 neurons,[7] tooth implants,[8] biomolecular probes,[9] protein folding,[10] the detection of DNA,[11] the detection of proteins and gene mutation,[12,13] tissue engineering,[14] the separation and purification of biological molecules and cells,[15] and for the identification of bacteria from clinical specimens.[16] They can also act as fluorescent biomolecules.[17]

Given the various applications of GNPs, they can also be applied to control the proliferation of cancer. It is known that the treatment of cancer continues to depend upon tedious and expensive treatments methods, such as chemotherapy, surgery, and use of anticancer drugs. To solve these problems in relation to cancer and to understand the anticancer efficacy of inorganic nanomaterials (NMs), new advances in nanobiotechnology have opened up new treatment possibilities. QDs and NPs of gold, which have very small diameters, have the capability to enter and target cells or microbes because the size of each cell is about ~20 µm. Cancer is a multifaceted process, where normal or positive cell propagation control is lost. Toward this direction, several reports have been published to demonstrate the utility of nanostructures against cancer cells. One such example was by Pan et al,[18] who describe the influence of the sizes of GNPs with different types of cells, namely epithelial, endothelial, phagocytes, and tissue stromal cells. They found comparative cytotoxicity levels of cells with GNPs when the sizes were altered.[18] El-Brolossy et al presented a photoacoustic technique, which determined the surface plasmon resonance of GNPs (dots and rods) and the absorption of NPs, which is the most appropriate and useful technique as compared to others.[19] PEG-coated GNPs of different sizes were utilized for radio-sensitization studies in HeLa cells. Apoptosis and cloning studies were also used to determine radiation effects.[20] Wahab et al reported the cytotoxic behavior of C2C12 cells at very low doses (100, 500, and 1,000 ng/mL) of GNPs; they sensitized the cells and showed that the growth of cancer cells was considerably affected by this treatment.[1] An endocytosis process was studied quantitatively with different sizes of GNPs in cancer cells, with the authors finding that GNPs ~45 nm in size exhibit improved drug delivery efficiency due to the higher uptake rate, whereas larger NPs were immobilized on the cell membrane to rebuild the cell morphology.[21] GNPs of different sizes have the ability to interfere with the maturation and the antitumor functions of dendritic cells, as induced by either lipopolysaccharide or heat-killed necrotic cancer cells.[22]

The tumor microenvironment is well recognized to play critical role in cancer progression and metastasis.[23] Glioblastoma multiforme (GBM) is the deadliest malignancy related to solid tumors and the central nervous system. Approximately 40% of all primary brain tumors are diagnosed in the form of a solid GBM mass with high infiltrative potential, explaining the poor survival rate. Even with standard treatment technology such as radiotherapy with chemotherapy to induce tumor cell death, the median survival period is still ~15 months.[24] Notably, GBM invades the brain itself but in the absence of homogenous spreading.[25,26] Thus, novel NP-based therapies are needed to prevent the spread and metastasis of solid tumor cells. Recently, we demonstrated the plasma-assisted delivery of GNPs to inhibit tumorigenesis by abrogating the PI3-AKT signaling axis.[27] Although several reports have been published in relation to the anticancer activity of NPs, the anti-spheroid and anti-invasiveness behaviors of NPs remain a major challenge of study. GNPs and QDs have drawn attention as modulators in the context of biological applications, and they exert a variety of functions depending upon the size, surface properties, and their interactions with cells. However, the possible role of QDs in solid-cancer spheroid growth inhibition remains largely obscure. Hence, targeting cancer spheroids by biocompatible multivariant-sized (MVS)-GNPs and QDs could be an attractive strategy to improve current anti-tumor treatments. We performed studies to investigate the anti-spheroid activity of various GNPs against human glioma cells and to determine whether this activity can be manipulated by these NPs depending on their properties. Using human glioma spheroids as a stem-like cells model, we showed that QDs inhibit growth and limit the degrees of brain cancer invasiveness, stemness, and progression. To understand the roles of QDs and NPs, here, we studied the anti-spheroid behaviors of MVS-GNPs and QDs against malignant stem-like cells. This study, for the first time, elucidates a novel gold quantum dot (GQD)-based anti-spheroid activity that promotes an anti-tumorigenic effect by modulating both tumor invasiveness and stemness.

Materials and methods

Synthesis of MVS-GQDs and GNPs

MVS-GNPs were synthesized with chemicals purchased from Sigma-Aldrich Co. (St Louis, MO, USA), which were used without further purification. In a typical experiment, concentrations from 1 to 4 mM (0.0393, 0.0786, 0.1179, and 0.1572 g) of chloroauric acid trihydrate ($HAuCl_4 \cdot 3H_2O$) were dissolved in 100 mL of double-distilled deionized water. The

pHs of these solutions vary; in this case the corresponding levels were 2.77, 2.80, 2.88, and 3.01. To reduce the salt of $HAuCl_4 \cdot 3H_2O$ for the formation of MVS-GNPs, we added 1% of trisodium citrate dihydrate ($N_3C_6H_5O_7$, 3 mM) to each solution. The pH levels of these solutions then increased to the range of 7.60–7.88. The colloidal solution was stirred robustly and refluxed at the boiling temperature for 15 minutes. As the concentration of $HAuCl_4 \cdot 3H_2O$ increased in the solution, a deep red solution of different size (DS)-GNPs was obtained. It was then cooled to room temperature and stored for further analysis.[1]

Characterization of MVS-GNPs

The crystallinity of the prepared MVS-GNPs was checked through the X-ray diffraction pattern (XRD; Rigaku, Japan) with $Cu_{K\alpha}$ radiation (λ=1.54178 Å) in the range of 20°–80° at a 6°/min scanning speed. To do this, the prepared colloidal solution was drop-casted onto a clean silicon substrate and then dried at room temperature for analysis by XRD. The general structural analysis was conducted via transmission electron microscopy (TEM, 200 KV, Jeol JSM 2010; Hitachi Ltd., Tokyo, Japan) equipped with high-resolution transmission electron microscopy (HR-TEM). For the TEM observations, an MVS-GNP pink-colored colloidal solution was sonicated for 10 minutes in a bath sonicator (40 KHz) beforehand. A carbon-coated copper grid was then dipped into it, and this was dried at room temperature for the morphological analysis.[1]

Cell culture and antibodies

Human solid cancer cell lines T98G, U87 and U373 glioblastoma cells, SNU-80 (thyroid cancer), H460 (lung cancer), MRC5 (normal lung fibroblast), and HEK293 (normal embryonic kidney cells) were established from the American Type Culture Collection (ATCC, Manassas, VA, USA)/Korean Cell Line Bank, Seoul, Korea. All the cells were maintained in DMEM (Hyclone, Korea) containing 10% FBS including antibiotics (100 U/mL penicillin, 100 µg/mL streptomycin containing an antimycotic solution) purchased from Thermo Fisher Scientific (Waltham, MA, USA). To obtain a spherical culture condition, GBM cells were collected after trypsinization and cultured in serum-free DMEM-F12 (Thermo Fisher Scientific) supplemented with 20 ng/mL of basic fibroblast growth factor (bFGF) (Sigma-Aldrich Co., St Louis, MO, USA), bEGF (Sigma-Aldrich Co.), B27 supplement (50X; Thermo Fisher Scientific), and antibiotics. Antibodies specific to E-cadherin (CDH1) and N-cadherin (CDH2) were purchased from Santa Cruz Biotechnology Inc. (Dallas, TX, USA). Antibodies specific to vimentin were purchased from Abcam (Korea). Antibodies specific to fibronectin were purchased from Cell Signaling Technology (Beverly, MA, USA), whereas β-actin was obtained from Sigma-Aldrich Co.

Plasmid DNA transfection

pCMV6 empty and pCMV6-XL5 (CTNNB1) vectors were purchased from Origene (Rockville, MD, USA) and transduced into the cells using Lipofectamine with Plus reagent (Thermo Fisher Scientific). After DNA transduction, the cell media were replaced with fresh media after 7–8 hour.

Metabolic viability and ATP measurements

Cell samples that were treated with MVS-GNPs or GQDs were checked for cytotoxicity with MTT–colorimetric assays. At the desired time points, 5 mg/mL MTT solution was added to each well and the plates were incubated for a further 3 hours, followed by the removal of the medium. The absorbance of purple formazan crystals precipitated in dimethyl sulfoxide was measured using a microplate reader (Synergy HT; Biotek; Winooski, VT, United States) at 540 nm, and the percentage viability value was calculated as described previously.[28,29] For the intracellular ATP level measurement, treated cells (2×10^5) were measured by EnzyLight™ ATP assays (Bioassays Systems, Hayward, CA, USA) according to the manufacturer's instructions. The luminescence levels were measured using a luminometer (Synergy HT; Biotek) with quantities relative to ATP standards.

Transwell assays for migration and invasion

To check the movement of the malignant cells, the cells were seeded into Transwell Boyden chambers (Corning Incorporated, Corning, NY, USA) with a pore size of 0.8 µm. Briefly, 2×10^4 cells were seeded in growth factor-reduced Matrigel-coated chambers with a serum-free medium. An FBS-containing medium was added to the lower chamber as a chemoattractant. After incubation at 37°C at the desired time point, invading cells were stained with a Diff-Quick kit (Thermo Fisher Scientific) and photographed. The extent of invasion was determined by counting cells in four microscopic fields in each well and was expressed as the average number of cells per microscopic field. For the migration assays, the Boyden chambers were left uncoated.

Flow cytometric uptake analysis

For cellular uptake measurements, after exposure to NPs, the cells were washed twice with PBS (Welgene, Korea),

followed by trypsinization, centrifuged at 1,000 rpm for 3 minutes, and further re-suspended in PBS. Afterward, the samples were analyzed immediately using a flow cytometer (FACSVerse; BD Biosciences, San Jose, CA, USA) with the FACS suite software. The side scattering parameter was used for the measurement of the intracellular NP uptake in the cells.

Western blot

After the treatment with the GQDs, the proteins were extracted from the cells using a lysis buffer (40 mM Tris–HCl [pH 8.0], 120 mM NaCl, 0.1% Nonidet-P40) supplemented with protease inhibitors. These proteins were separated by SDS-PAGE and then transferred to a nitrocellulose membrane (Amersham, Chicago, IL, USA). The membrane was incubated with primary antibodies overnight at 4°C followed with a peroxidase-conjugated secondary antibody. Targeted proteins were visualized by enhanced ECL procedures (Amersham) according to the supplier's protocol.

RNA extraction and real-time PCR

Total cell RNA from samples was isolated using the Trizol reagent (Thermo Fisher Scientific) manually. All reactions were performed using a KAPA SYBR FAST qRT-PCR kit (KAPA Biosystems, Wilmington, VA, USA) in a Rotor Gene Q thermocycler (Qiagen NV, Venlo, the Netherlands), and the results were expressed as the fold change.

Self-renewal behavior test

For the sphere-forming assays, glioma spheroids were seeded into low-attachment cell culture dishes. Treated and untreated spheres were checked under a phase-contrast microscope and were photographed. The sizes of the spheres were measured using Motic Images Plus software, and the data were represented as the mean of the average size of spheres chosen from three independent fields. The numbers of spheres formed in both the groups were counted under the phase-contrast microscope in three randomly chosen fields until day 4. Results were expressed as the average number of spheres.

Immunocytochemistry

To visualize the N-cadherin (CDH2) expression levels, treated cells were fixed with 4% paraformaldehyde and permeabilized with 0.1% Triton X-100 in PBS. Afterward, the cells were incubated with the unconjugated mouse polyclonal N-cadherin antibody (1:200) in a blocking buffer (PBS with 1% BSA and 0.1% Triton X-100) at 4°C overnight. Stained cells were visualized using anti-mouse Alexa Fluor 488 (Thermo Fisher Scientific). Cell nuclei were detected using DAPI (Sigma-Aldrich Co.). Stained cells were pictured with a fluorescence microscope (Olympus IX71; Olympus Corporation, Tokyo, Japan).

Analytical determination of MVS-GNPs

The analytical determination and validation of the concentrations of MVS-GNPs (1 μg/mL) against cancer and normal cell suspensions were conducted with statistical analytical techniques. The absorbance was measured at λmax 500 nm as determined by a UV-visible spectrophotometer. In statistical analysis, quantitative and qualitative determination of GQDs (NPs) have shown binding properties with biological specimens. MVS-GNPs were calibrated with analytical balances which provided resulting concentration for method accuracy and precision, recognized to purity. The linear calibration graph was constructed for GNPs by plotting absorbance against concentration (concentration 0.5–2.5 μg/mL), which provided linearity and optical regressive data. The satisfactory data obtained from absorption spectra (in the term of absorbance) and absorbance of GQDs (NPs) depend upon UV-visible spectrum. Therefore, all measurement results were recorded at wavelength 500 nm and established by UV-visible spectrophotometer. The empirical formula provided more constant values to ensure that they are fit for the proposed method. An optimization and validation method was applied to verify whether the method works reliably in their hands. The GQD NPs is common way for analytical method, which gives standard sample against many factual variables factors such as concentration, volume, pH, time, and temperature. The optimized and validated sample experimental conditions (pH, concentration, volume, time and temperature),the optimized concentrations of MVs-GNPs are employed to control the cells. The concentration of analyte is directly proportional to the sample solutions and result data's obtained by analytical procedure. The validation parameters were used to determine the accurate concentration of the analytes or sample solution which was calculated from the statistical parameters such as linearity, limits of detection, quantitation, precision, and accuracy as per guidelines of International Conference of Harmonization (ICH).

Statistical analysis

Resulting data values are expressed as the mean ± SD of triplicate measurements. Statistical analyses were performed using parametric two-tailed, unpaired Student's *t*-tests by using GraphPad Prism software, version 7.0. Significance was defined as $*P<0.05$, $**P<0.001$, and $***P<0.0001$

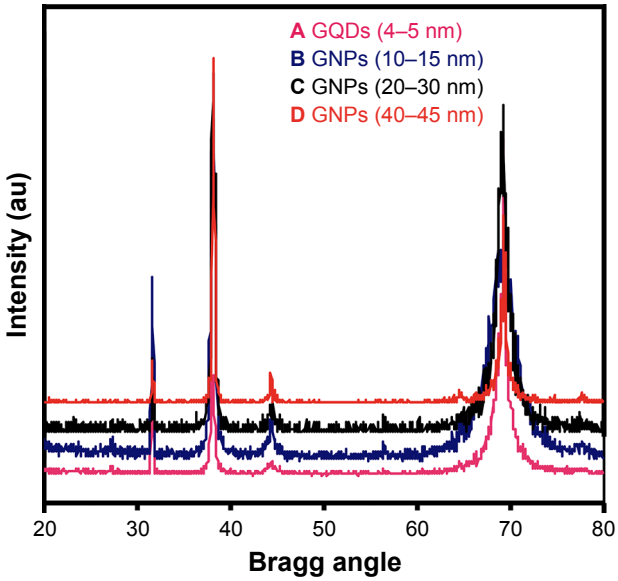

Figure 1 X-ray diffraction patterns of DS-GNPs.
Note: (**A**) GQDs (4–5 nm), (**B**) GNPs (10–15 nm), (**C**) GNPs (20–30 nm), (**D**) GNPs (40–45 nm).
Abbreviations: GQD, gold quantum dot; GNP, gold nanoparticle.

compared with the controls. Non-significance is denoted as NS.

Results

XRD analysis of MVS-GNPs

The crystallinity and phases of the prepared MVS-GNPs were analyzed with the XRD patterns, as presented in Figure 1A–D. Observed three distinct peaks in the XRD outcomes, with two major peaks related to the GNPs at 2θ =38.17 and 44.45, whereas the peak at 31.7 denoted the silicon substrate used. All the peaks except for silicon correspond to the standard diffraction pattern of gold with a face-centered cubic structure (JCPDS No 04-0784). The broadening of the X-ray peaks is primarily due to the very small particle size of the gold. The slight shift in the peak position indicates the presence of strain in the crystal structure, which is a characteristic of nanocrystallites of this size.[1,30]

Morphological analysis of the synthesized MVS-GNPs

The general morphology of MVS-GNPs was investigated via HR-TEM and the selected-area electron diffraction pattern. Characteristic TEM images were recorded via the deposition of a colloidal solution of MVS-GNPs onto carbon-coated copper grids, as shown in Figure 2. The obtained TEM image clearly indicates that several small particles are present. After the detailed study, the size of each particle was estimated to be <10 nm (Figure 2A). The size distribution of the QDs was also measured with the use of the ImageJ software package, which showed that the size of each QD is about 4.34 nm (Figure S1). The general structural morphology of each particle appeared to be spherical, and the particles were free from agglomeration. The representative picture shows the general morphology and the crystallinity of the material side by side via HR-TEM imagery (Figure 2B). The HR-TEM image in Figure 2B demonstrates the crystalline characteristic of the particles, which are ~0.233 nm in size, equal to the face-centered cubic structures of the gold particles.[1]

Figure 2C shows that the sizes of NPs range from 10 to 15 nm and that they are nearly spherical in shape. In our experiment, as the concentration of chloroauric acid trihydrate ($HAuCl_4 \cdot 3H_2O$) increases in the solution, the sizes of the NPs also increase, as evident from the TEM images. The particles have a rough surface, are crystalline, and are well separated without agglomeration. As indicated in the TEM image in Figure 2C, the prepared colloidal structures are highly dense. The HR-TEM image in Figure 2D clearly demonstrates the crystal lattice, which shows the crystalline characteristic of the grown particles. The size is close to ~0.235 nm, equal to the face centered cubic of GNPs and consistent with previous findings.[1] As the concentration of the precursor increases in the solution, the size of the particles also increases in proportion. Figure 2E shows that the average diameter of each particle is in the range of ~20–30 nm. Here, the spherical shape of the NPs is well arranged, as observed in the TEM micrograph in Figure 2E. The lattices between the fringes are also well separated at distances of ~0.234 nm (Figure 2F). Higher or increased concentrations of the precursor of the colloidal solution form finer particles which are aggregated, and as the size increases, giant crystals of NPs are formed. The crystallinity of the particles also changes, which can be seen in the HR-TEM and XRD results (Figure 1). As the samples are heated with increased amounts of the precursor solution, modifications of the NP shapes occur randomly, namely spherical or triangular, and ellipsoidal as well as circular forms about 45–50 nm in size (Figure 2G). At higher concentrations, agglomeration of the finer particles begins, leading to larger NPs, as shown in Figure 2G. Under other processing condition, the NP size reaches ~20 nm with a morphology similar to the previous finding. The small NPs aggregate and form larger particles due to the increased concentration of the material. The sizes of the NPs increase to ~45–50 nm, as is clearly evident in the TEM observation (Figure 2G). At higher concentrations (4 mM; upon boiling for 15 minutes), the NPs are highly aggregated with each

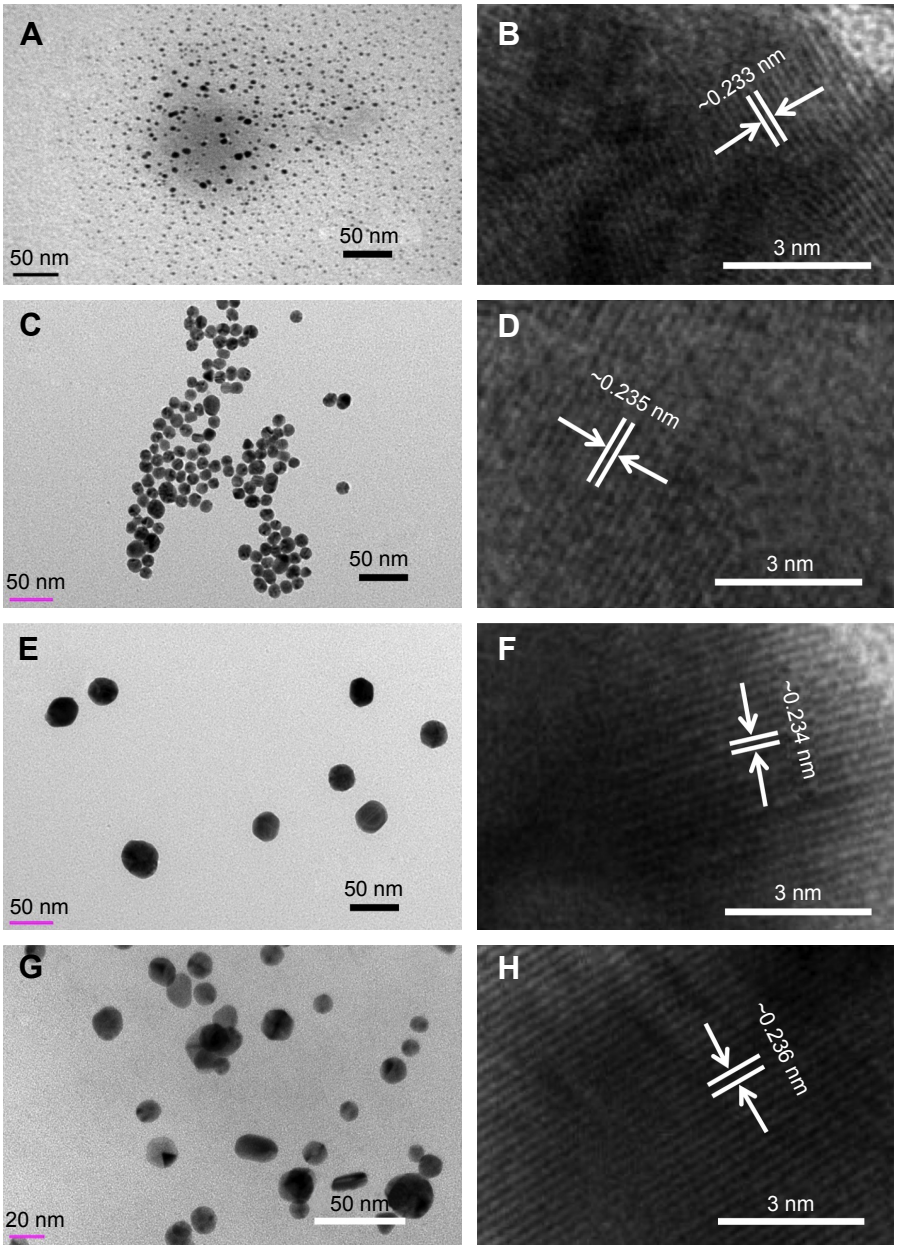

Figure 2 MVS-GNP images of synthesized GQDs and GNPs.
Notes: (**A**, **C**, **E**, and **G**) show the various sizes of the GQDs: (**A**, <10 nm) and GNPs (**C**, **E**, and **F**, 10–15, 20–30, and 45–50 nm, respectively), whereas (**B**, **D**, **F**, and **H**) show HR-TEM images depicting the differences between the two lattice fringes, which are in the range of ~0.233 to ~0.236 nm, respectively. The HR-TEM observations indicate the crystallinity of the synthesized products.
Abbreviations: GQD, gold quantum dot; GNP, gold nanoparticle; HR-TEM, high-resolution transmission electron microscopy.

other and form a larger structure (~45–50 nm) (Figure 2G). The HR-TEM images display the lattice with a well-arranged form of the larger NPs (~45–50 nm), which are ~0.236 nm in size. The observed data are clearly consistent with the XRD pattern of the grown materials (Figure 1).

Statistical analysis to resolve MVS-GNPs with normal and cancerous cells

Analytical methods were used for the purpose of regulating cancerous and non-cancerous cells, involving the MVS of GNPs (H-460, HEK293, MRC-5, SNU-80, and T98G). The statistical parameters provided more rigorous data for considerations of quantitative and qualitative analyses. The proposed method was used to determine the concentration range of the GNPs, ultimately to control the growth of cancerous cells. The absorption spectra of GNPs were recorded with a UV-visible spectrophotometer in the form of absorbance at a wavelength of 500 nm, as indicated in Figure S2A–D. This indicates that the absorbance of the sample solution is proportional to the number of absorbing molecules in the spectrometer

light beam. In addition, the presence of much variation was noted in the recorded range of the GNPs (concentration 0.1–0.5 μg/mL) from the linear calibration graph (Beer's law), as shown in Figure S2A–D. The linear graphs which plot the absorbance against the concentration show linear lines were fitted into the linear regressive equations, resulting in excellent correlation coefficients (r^2), as shown in Figure S3A–D.[1] The linear range exposed relationship between NM and sample concentration which shows significant regression equation data or straight line graph as shown in Figure S3A–D. Generally, the most important variance parameters are the range, SD, and variance of the calibration line, which are useful as preliminary descriptive statistics. The four calibration graphs represent the MVS-GNPs (GQDs, GNPs-10, GNPs-25, and GNPs-50, correspondingly) introduced with normal and cancerous cells (H-460, HEK-293, MRC-5, SNU-80m, and T98G cells). All of the distinguished values are arranged in Tables S1–S4 for the same instrumental response for consideration of each optical parameter. The reliable resulting data exposed the ranges of molar absorptivities (Є) and variances (GQDs: 0.291×10^3 – 0.628×10^3 L $mol^{-1}cm^{-1}$; G-NPs-10: 0.141×10^3 – 0.524×10^3 L $mol^{-1}cm^{-1}$; G-NPs-25: 0.130×10^3 – 0.448×10^3 L mol^{-1} cm^{-1}; G-NPs-50: 0.114×10^3 – 0.588×10^3 L $mol^{-1}cm^{-1}$), variance (S_0^2) range (G-QDs: 4.494×10^{-6} – 4.426×10^{-4}; G-NPs-10: 4.376×10^{-5} – 5.271×10^{-4}; G-NPs-25: 2.621×10^{-5} – 3.115×10^{-4}; G-NPs-50: $2.4\,47\times10^{-5}$ – 5.094×10^{-4}). The limit of detection (LOD) and limit of quantitation (LOQ) values of the GNPs were established at the minimum concentration levels while monitoring the lower to higher values of the LOD and LOQ (μg/mL) of the GQDs (0.012–0.165 to 0.036–0.525), the GNPs-10 (0.133–0.292 to 0.404–0.884), the GNPs-25 (0.116–0.408 to 0.352–1.236), and the GNPs-50 (0.203–0.459 to 0.605–1.391) samples. Therefore, the resulting data were assessed in an adequate manner to ensure that the reliable statistical values are acceptable at a significant level (Tables S1–S4). As per the guidelines of the ICH, the optimization method and validation of the parameter performances support the feasibility of the analytical methods. The optimization process involves an analytical method that uses a standard sample in presence of many realistic variables. The ICH guidelines clearly demonstrate the imperative to regulate publications on analytes.

QDs decrease spheroid cell growth with a decline in ATP levels

Many earlier studies suggest that cancer stem cells (CSCs) are highly resistant to conventional radiotherapy and chemotherapy treatments and that there are subpopulations of cancer tissues.[31,32] In agreement with these studies, we initially investigated the effects of GQDs and GNPs on the growth of U87MG and U373MG glioma cells in spherical cultures. The data indicated that GQDs (<5 nM) have greater inhibitory efficacy on both deadly and aggressive glioma spheroids in a concentration-dependent manner as compared to GNPs at all tested concentrations (Figure 3A and B). Moreover, ATP is widely considered as a primary source of energy in cancer cells, and enhanced levels of ATP compromise a potential marker for cell growth.[33] Next, we investigated the impact of MVS GNPs and GQDs on the metabolic programming of brain-cancer stem-like U87 and U373 cells at a 50 nM concentration. Interestingly, GQDs decreased the ATP content of brain spheroids by >30% after 24 hours of treatment, whereas GNPs did not alter ATP levels significantly (Figure 3C and D). These results demonstrate that reduced tumor-ATP levels in glioma spheroid cells inhibit the growth of these resistant cells with GQDs.

QDs potentially reduce the motility and phenotypic changes of glioma cells

The epithelial–mesenchymal transition (EMT) plays a crucial role in cancer relapse and secondary tumor progression. During this process, cells lose their polarity and enter into contact adhesion with adjacent epithelial cells. They also gain mesenchymal behavior, such as motility.[34] To this end, we performed migration and invasion assays in a 2D system using Transwell Boyden chambers. Our data showed that treatment with GQDs at a 100 nM concentration significantly reduced the migration and invasion capabilities of U87MG glioma cells as compared with untreated control cells (Figure 4A and B). As the loss of the epithelial marker e-cadherin (CDH1) and the gaining of the mesenchymal markers n-cadherin (CDH2), fibronectin (FN), and vimentin (VIM) expression are the primary hallmarks of EMT toward tumor relapse during progression, we screened the expression levels of these markers in U87MG glioma cells. Immunoblot and PCR analyses showed significant upregulation of CDH1 along with the suppression of CDH2, FN, and VIM in glioma cells (Figure 4C and D). In addition, localization of the CDH2 expression level was weaker on the cell membrane after the treatment with GQDs in glioma cells, similarly, as confirmed in the PCR and Western blot analyses (Figure 4E). These results suggest that GQDs inhibited the mesenchymal phenotypic properties with the reversal of EMT.

QDs promote anti-self-renewal efficiency in brain-stem-like populations

CSCs are also known as tumor-initiating cells with stem-cell-like properties.[35,36] The acquisition of stemness by cancer cells

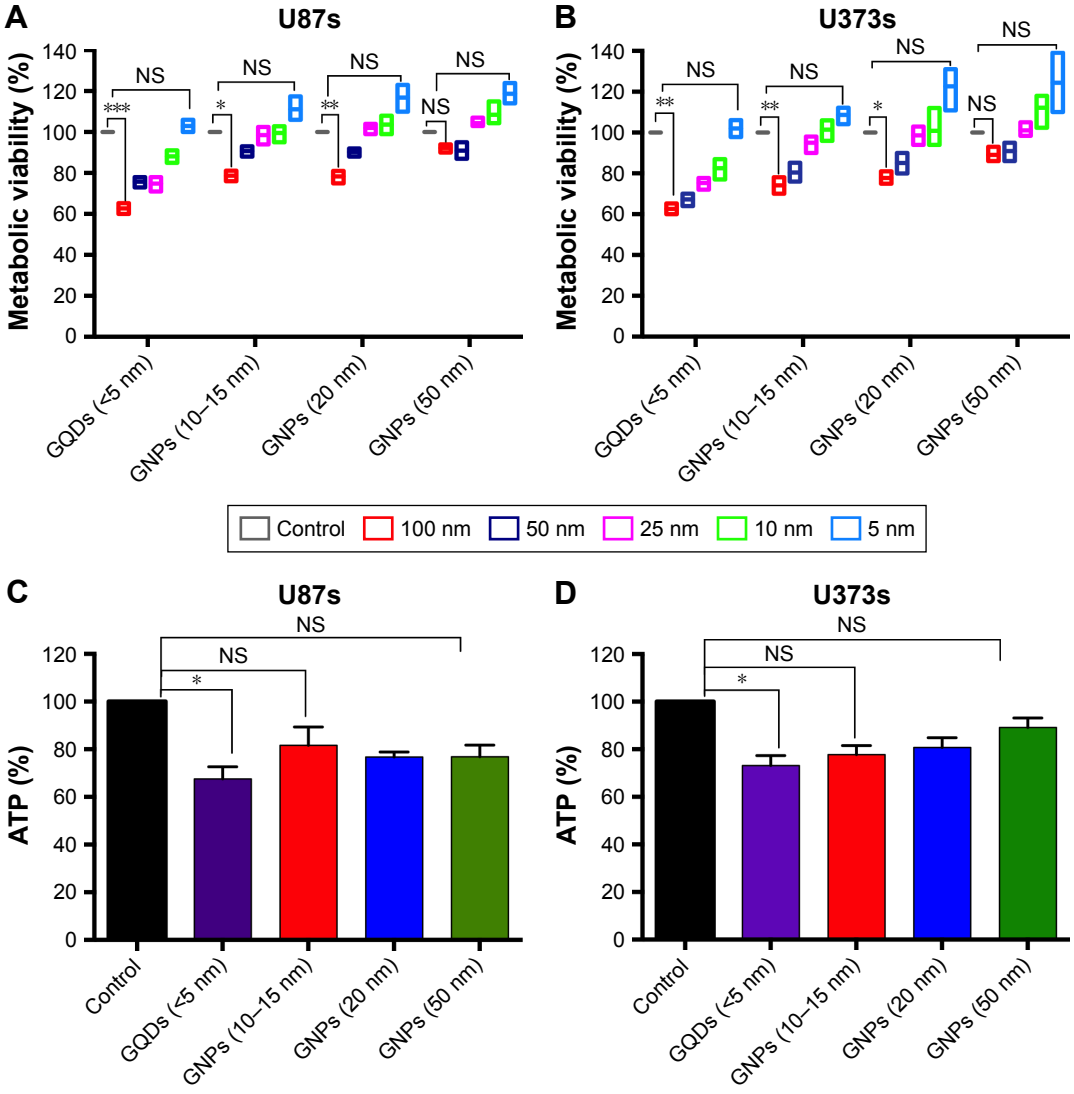

Figure 3 GQDs suppress the viability of glioma spheroids more efficiently than GNPs.
Notes: (**A** and **B**) MTT viability assays of U87 and U373 glioma spheroids, respectively. Viability was measured at 24 hours after a treatment with various sizes of GQDs (<5 nm) and GNPs (10–50 nm) at different concentrations (5–100 nM). (**C** and **D**) Intracellular ATP measurements in U87 and U373 glioma spheroids, respectively, with treatment with various sizes of GQDs and GNPs at a 50 nM concentration at 24 hours. Significance was calculated compared to controls and these levels are presented as *P<0.05, **P<0.01, and ***P<0.001. Nonsignificance is denoted as NS.
Abbreviations: GQD, gold quantum dot; GNP, gold nanoparticle.

occurs via the process of EMT and the simultaneous gain of an invasive mesenchymal phenotype.[37,38] It is also believed that EMT is involved in the acquisition of certain CSC properties, such as the formation of tumorospheres capable of self-renewal and the expression of stem-cell-like markers.[39] To determine whether the GQDs inhibited the CSC characteristics of U87MG glioma cells in a sphere-culture condition, we conducted a sphere-formation ability test in ultra-low attachment dishes and found that sphere formation was significantly decreased in U87MG cells exposed to GQDs when compared to untreated cells (Figure 5A and B). Moreover, when the expression levels of stem-cell-like markers of CD133, OCT4, SOX2, Nestin, Musashi1, and β-catenin (CTNNB1) were analyzed in the same spheroid cells, a remarkable reduction was noted in the spheroids treated with GQDs, comparable to untreated cells (Figure 5C and D). Given that CD133 expression levels are highly enriched in brain-stem-like cells, an additional The Cancer Genome Atlas data set analysis using an online tool (http://www.betastasis.com/glioma/tcga_gbm/two_gene_scatterplot_affymetrix_human_exon_10_st/) was performed, showing stronger outcomes than our findings in that CD133 and CTNNB1 were positively correlated with each other in glioma cases (Figure 5E). These results provide evidence that G-QDs have the potential to hinder the self-renewal ability, with a subsequent loss of stem-cell-like markers as well in glioma spheroids.

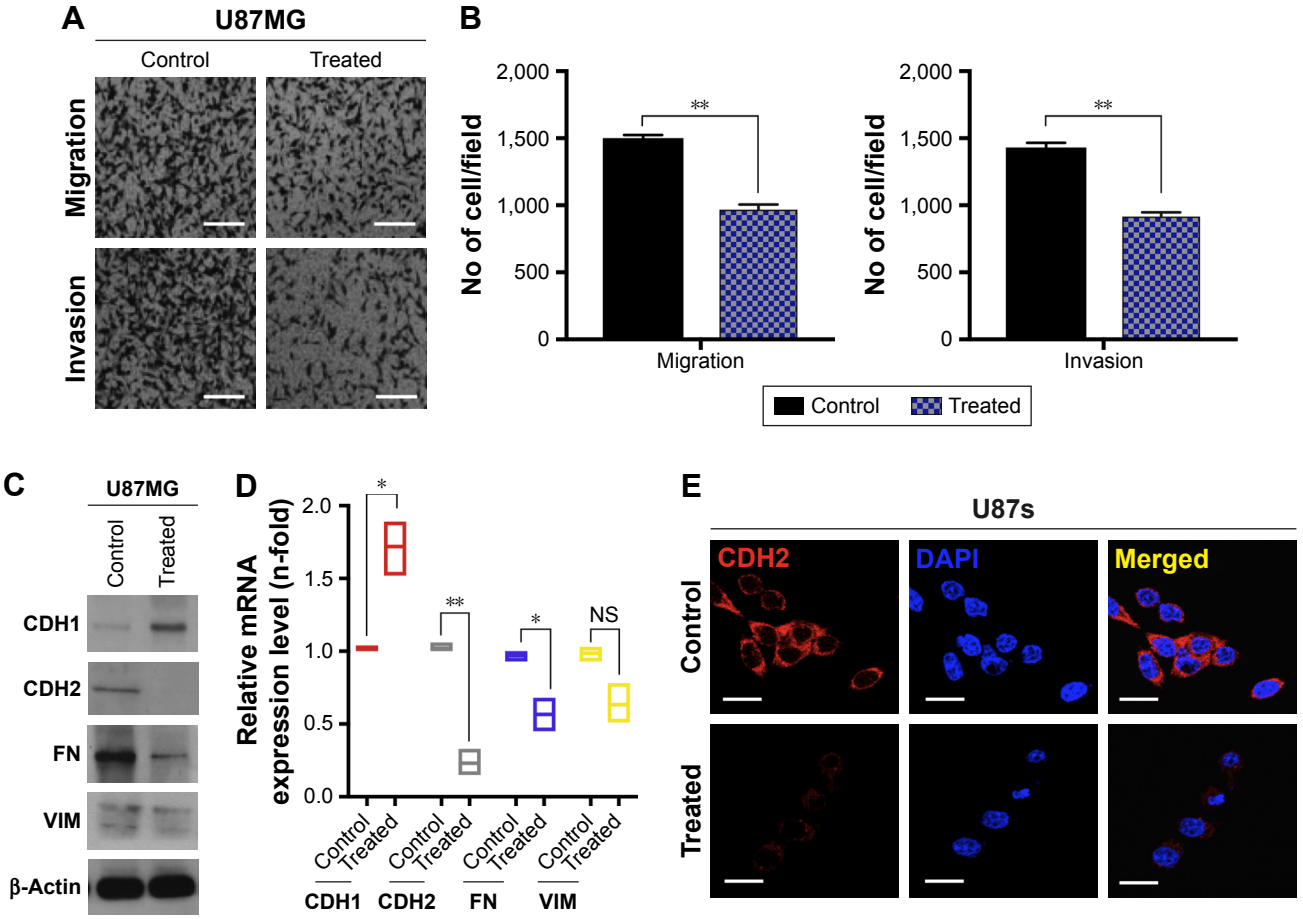

Figure 4 GQDs decrease the aggressiveness of glioma cells.

Notes: (**A** and **B**) 2D migration and invasion assays were performed in U87 cells via Transwell assays stained at 24 hours after a treatment of <5 nm GQDs at a 100 mM concentration. (**C** and **D**) Immunoblotting and RT-qPCR detection for EMT markers, in this case e-cadherin (CDH1), n-cadherin (CDH2), fibronectin (FN), and vimentin (VIM) in <5 nm G-QDs under conditions identical to those described above in U87 glioma cells. β-Actin was used as a control for normalization. (**E**) Expression levels of CDH2 were visualized by immunofluorescence staining. Typical images of <5 nm GQDs (100 nM) treated and untreated in identical glioma cells were photographed at 20× magnification. Scale bar =10 μm. Significance levels were calculated compared to the controls and are presented as $^{*}P<0.05$, $^{**}P<0.01$, <0.001. Nonsignificance is denoted as NS.

Abbreviations: GQD, gold quantum dot; GNP, gold nanoparticle; EMT, epithelial–mesenchymal transition.

Enhanced β-catenin expression in glioma cells promote the tumorigenic potential with CSC maintenance

It was demonstrated in earlier reports that β-catenin and the CTNNB1 signaling pathway play roles in the tumorigenesis of various human cell types and in the regulation of the CDH1/CTNNB1 complex frequently linked to EMT.[40] To determine the importance of CTNNB1 in glioma cell progression along with CSC population maintenance, we checked the viability of glioma cells after CTNNB1 overexpression. Of note, CTNNB1-overexpressed cells blocked the effect of GQDs on the suppression of glioma cell growth when compared to GQD cells treated in the presence of an empty vector (Figure 6A). Importantly, U87MG spheroid cells overexpressing CTNNB1 showed enhanced sphere-forming ability in cells treated with GQDs (Figure 6B). Similarly, CTNNB1-overexpressed cells blocked the effect of GQDs to suppress glioma migration, and CDH2 mesenchymal marker when compared to GQDs treated cells in the presence of an empty vector. Restoration of CDH1 was also dropped in GQDs cells after CTNNB1 overexpression (Figure 6C and D). These results strongly support the assertion that β-catenin is essential for the repression of self-renewal, with subsequent EMT progression in glioma cells.

Discussion

The present study demonstrates the formation of QDs and MVS-GNPs through colloidal process. For this, $HAuCl_3{\cdot}3H_2O$ was used at different concentration levels, and to these mixture, $N_3C_6H_5O_7$ was incorporated at a fixed concentration (3 mM). Variant size particles (below 10–50 nm) were

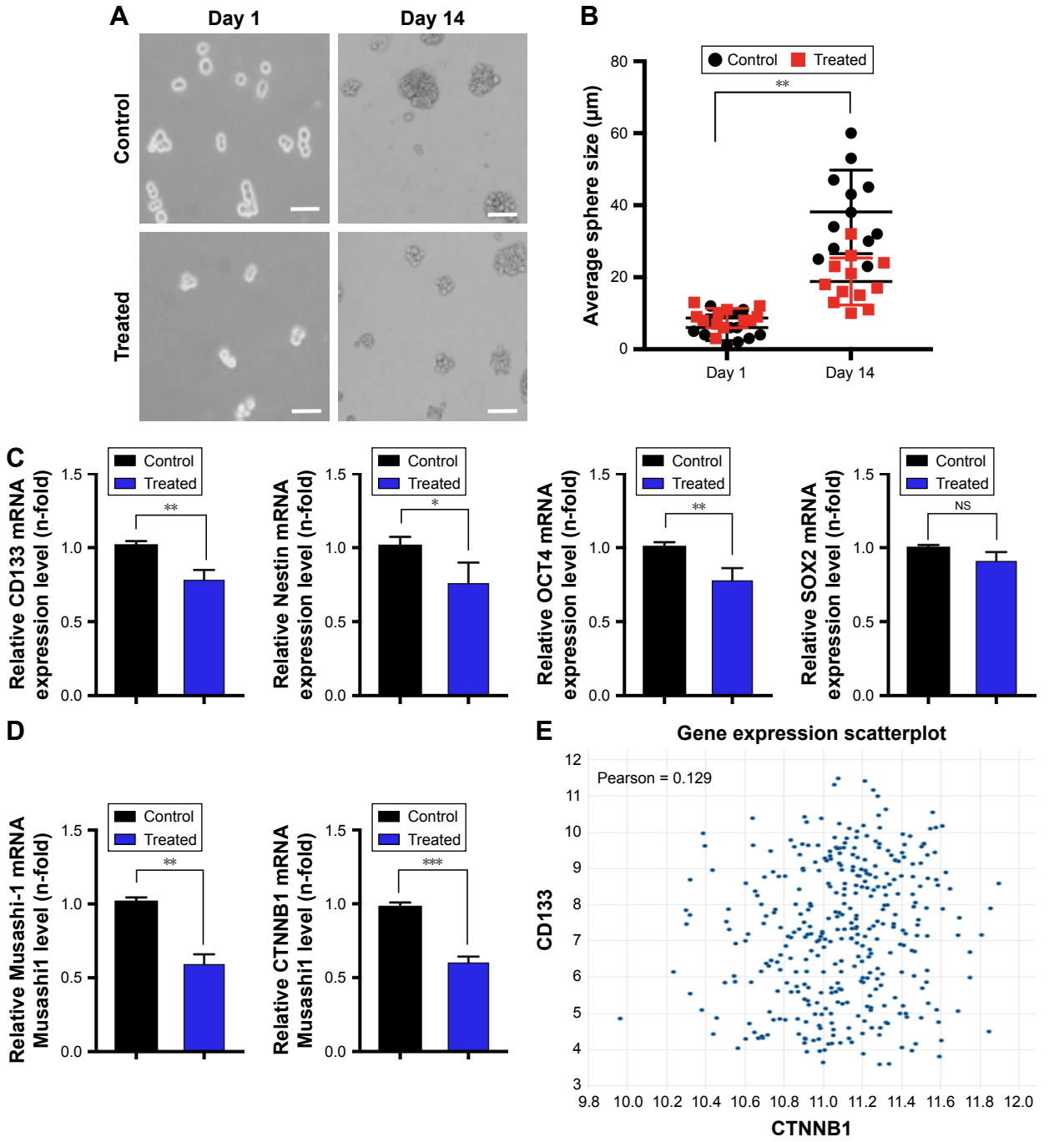

Figure 5 The self-renewal ability was inhibited after exposure to GQDs in glioma spheroids.

Notes: (**A** and **B**) A sphere-forming assay was performed until 0–4 days 24 hours following a treatment of <5 nm GQDs at a 100 nM concentration in U87 glioma spheroids. The representative graph shows the size of the formed spheres after the treatment according to Motic Images Plus software. (**C** and **D**) RT-qPCR analysis outcomes of stem-cell-like markers of CD133, OCT4, SOX2, Musashi-1, Nestin, and β-catenin (CTNNB1) in treated and untreated spheroids in panel A. β-Actin was used as a control for normalization. (**E**) Co-relation analysis results of CD133 (highly expressed specifically in glioma stem cells) and CTNNB1 using a publically available TCGA data set online tool. Scale bar =100 µm. *P<0.05; **P<0.01; ***P<0.001. Nonsignificance is denoted as NS.

obtained and characterized through XRD. The general morphologies and their crystalline character were defined via TEM equipped with HR-TEM correspondingly. The statistical analytical parameters of the LOD, LOQ, and SD were applied to determine the detailed interaction between the QDs and the DS-GNPs. The known concentration of GNPs can be used to diagnose normal and abnormal cells, which was done here to reduce the toxicity as a chemico-friendly analytical standard solution method. The suspension solution study led to admirable results, showing significance given the use of multivariate techniques, which have underlying assumptions and restrictions. The important statistical

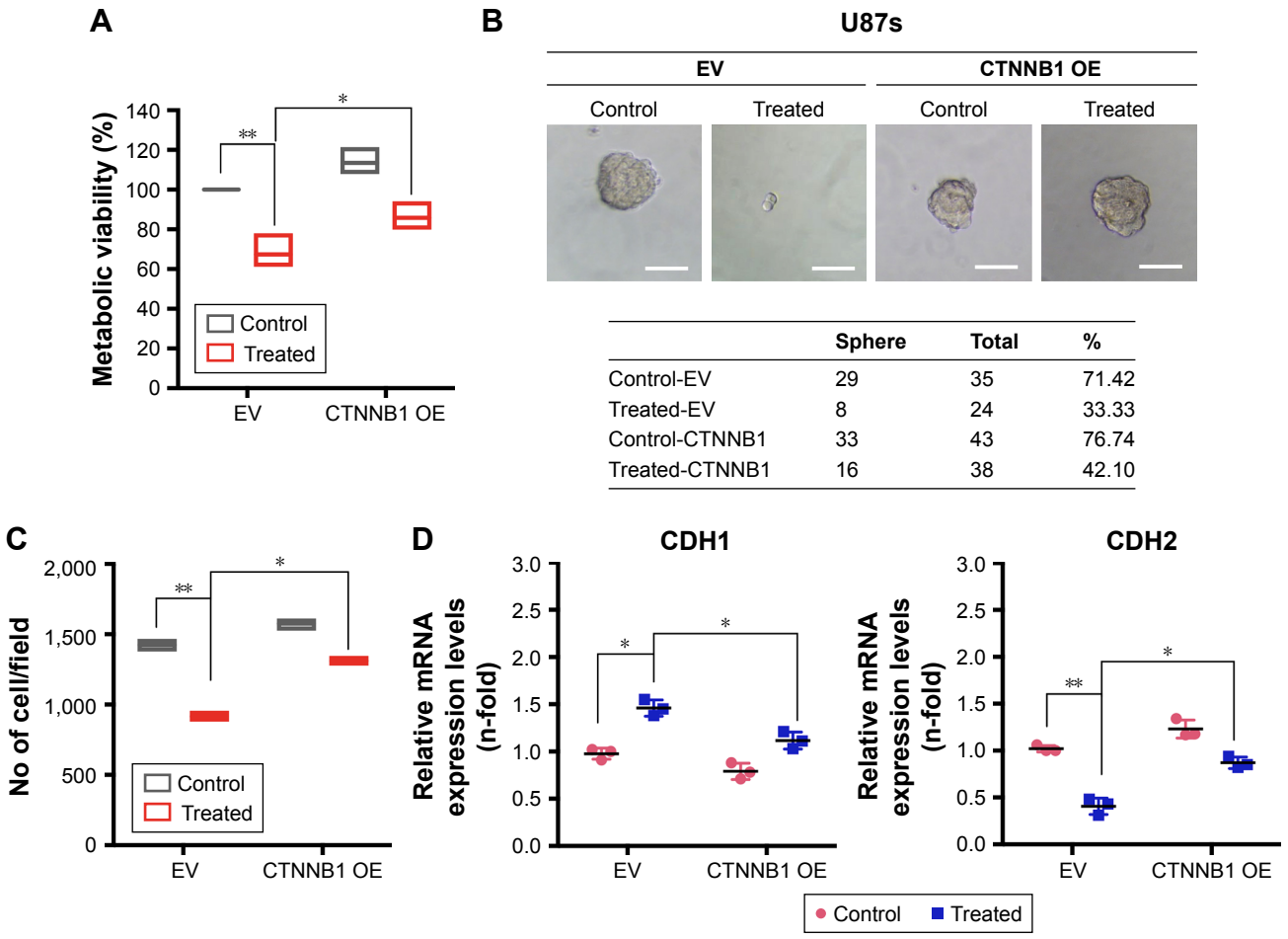

	Sphere	Total	%
Control-EV	29	35	71.42
Treated-EV	8	24	33.33
Control-CTNNB1	33	43	76.74
Treated-CTNNB1	16	38	42.10

Figure 6 β-Catenin overexpression diminished the effect of GQDs on the reduction of malignancy in glioma spheroids.
Notes: (**A**) Viability of U87s glioma spheroids after EV (pCMV6 empty vector) and pCMV6-XL5 (CTNNB1) overexpression. (**B**) Sphere-forming assay of U87s glioma spheroids after EV and CTNNB1 overexpression. The table shows the total number of spheres which formed after each treatment. (**C**) Migration of U87 glioma cells after EV CTNNB1 overexpression. (**D**) RT-qPCR of U87 glioma cells after EV and CTNNB1 overexpression. <5 nm GQDs were treated at a 100 nM concentration in each panel and a similar treatment condition was maintained throughout all experiments. β-Actin was used as a control for normalization. Scale bar =20 µm. *$P<0.05$; **$P<0.01$; Nonsignificance is denoted as NS.
Abbreviation: GQD, gold quantum dot.

parameters are mean, SD, variance, linear regression analysis, concentration range, LOD, and LOQ. The aspects of qualitative and quantitative study express statistical identification of the NMs. The qualitative and quantitative aspect is very sensible to determine outstanding statistical identification of analyte (NMs) and statistical parameters suitability was confirmed by validation characteristics. The validation parameter outcomes correspond to the acceptance criteria of the data results (as indicated in the figures and tables). Therefore, the parameter results make it easier to determine and clarify the sufficient amounts of NMs used in the target cells. Frequently, the linearity was appraised by the graphical response (Figure 2A–D). All of these graphs were plotted with the relative responses on the y-axis and with the corresponding concentrations on the x-axis, on a log scale, resulting in a straight line between both the axes. Five points of linear lines are recommended for five concentrations of GNPs (µg/mL), with the lower concentration point to the higher concentration point providing the range (Beer's law =0.5–2.5 µg/mL) of the analyzed standard solution. The measured range was defined in relation to the analyte, which is directly proportional to the GNPs used (NMs). The tangible data points were then fitted to best straight line to generate the slope, intercept, and correlation coefficient from the linear regression equation (A=a+b C). For the mathematical calculation, the Origin (ver. 6.1) software was used, and the significant results are summarized for all data points (Tables S1–S4). According to the general rule, the value of the correlation coefficient can be designated as $0.90<r<0.95$, meaning a fair calibration curve, with $0.95<r<0.99$ for a good curve and $r=0.999$ (highest value) for a high-quality calibration curve with excellent linearity. In relation to this, the absorbance of

the GNPs (GQDs) is associated with cancerous cells, and the molar absorptivity (Є) values were indicating high sensitivity of the GQDs. The limits of the intercept ($\pm ts_a$) and slope ($\pm ts_b$), the variance (So^2) of the calibration line, LOQ, and LOD were calculated at 95% confidence level. Regarding to size of NPs with sequencing manner (G-QDs, G-NPs-10, G-NPs-25 and G-NPs-50), each NP was analyzed separately due to distinguish absorbance data recorded by a UV-visible spectrophotometer. The adequate data are presented in Tables S1, S2, S3, and S4.

In a recent study, surface-charge- and size-dependent cellular associations of GNPs with human cells were investigated using flow cytometry techniques. Recent reports showed that the measured side scattering (SSC) intensities while using the flow cytometry method are linearly related to the cellular association of the GNPs as well as the core sizes of the GNPs.[41] In comparisons between inductively coupled plasma mass spectrometry and flow cytometry results on human cells, researchers found linear correlations between the cellular GNPs and the SSC intensities as measured by flow cytometry and used them to estimate the amounts of GNPs associated with cells. Using this validated technique, comparisons with the SSC intensities of glioma cells exposed to four different types of GNPs (Figure S4) were performed. It was observed that the uptake of NPs by a glioma cell culture depends on the sizes of the NPs. GQDs and NPs 15 nm in size showed greater uptake levels as compared to other NPs. The uptake difference in the NPs may explain the high bioactivity against glioma cells. In fact, particles with smaller dimensions exhibit low density and high quantity levels, which easily facilitates their accumulation in U87 and U373 spheroid cells and affects their viability.

Here, when we screened the synthesized GNPs, we found that they have a greater effect on reducing the growth of CSC-like populations in tumor cells with disturbances in intracellular ATP levels (Figure 3). Among them, remarkably, a treatment with GQDs reduced the aggressiveness of glioma cells (Figure 4). These highly resistant CSCs limit the efficacy of chemotherapy/radiotherapy in terms of tumor mass reductions. Moreover, we observed that in U87 glioma spheroid cells, treatment with GQDs decreased the self-renewal properties, resulting in a loss of stem-cell-like marker expression levels. Interestingly, the expression of CD133 was reduced by a greater level, sufficient to indicate that glioma spheroid cells lose their potential to increase stem-like cell populations (Figure 6). GQDs directly inhibit the EMT process and abrogation in stem cells. To understand this mechanism, we found that CTNNB1 signaling was mainly disrupted after a GQD treatment in glioma spheroid cells. It is important to note that the CTNNB1 expression level is also enriched in glioma stem-like cells, which was subsequently suppressed after the GQD treatment. Overall, an approach to inhibit cancer stemness and EMT in solid cancer cells by abrogating the β-catenin signaling pathway using MVS-GNPs is a promising way to improve patient survival. The obtained results indicate that the GQDs could be useful as a cancer treatment to control cancer spheroid cell progression and maintenance. Collectively, our data indicate the potential roles of MVS-GNPs at low doses against solid cancer progression, initiation, and maintenance.

Conclusion

It is concluded that the operationalized tentative data gleaned via a statistical analytical method provided specific, precise, linear, accurate, sensible, and satisfactory results regarding the concentration of GNPs quantified by statistical parameters for maximum control of cancerous cells. All applied statistical parameters are validated under the guidelines of the ICH. The absorbance levels of two distinguishable structures of gold NMs (QDs and NPs) of different sizes (GQDs [<5 nm], GNPs-10 nm, GNPs-25 nm, and GNPs-50 nm) were measured at the same wavelength (500 nm). Small GQDs showed significantly more attraction toward cancerous cells and expressed high absorbance as compared to larger GNPs at 50 nm.

Gliospheres cannot be treated by radiotherapy and chemotherapy due to their highly resistant properties and self-renewal characteristics. We attempted to target a CSC-like population with MVS-GNPs within glioma cells and to monitor changes in mesenchymal traits. In summary, our data indicated that GQDs are NPs with good biocompatibility, and they can have a cytotoxic effect on tumor spheres at maximum concentrations, which are safer for normal cells. Treatment with these GQDs significantly reduced the sphere-forming ability of glioma spheroid cells. GQDs can exploit the interaction between E-cadherin and CTNNB1 and deliver a maximum inhibitory effect to tumors as compared to the level currently possible with present therapeutic methods. Our results provide evidence that GQD NPs can serve as a target drug delivery system to brain-stem-like cells.

Acknowledgments

This study was financially supported by the King Saud University, Vice Deanship of Research Chairs. This work was supported by a grant from the National Research Foundation of Korea (NRF), which is funded by the Korean Government, Ministry of Science, ICT and Future Planning (MSIP)

NRF-2016K1A4A3914113 and NRF-2016R1C1B2010851. This work is also supported by Kwangwoon University Research Grant in 2018–19. This research was also supported by the Bio & Medical Technology Development Program of the NRF funded by MSIP (No-2017M3A9G8084539).

Disclosure

The authors report no conflicts of interest in this work.

References

1. Wahab R, Dwivedi S, Khan F, et al. Statistical analysis of gold nanoparticle-induced oxidative stress and apoptosis in myoblast (C2C12) cells. *Colloids Surf B Biointerfaces*. 2014;123:664–672.
2. Goharshadi EK, Sajjadi SH, Mehrkhah R, Nancarrow P. Sonochemical synthesis and measurement of optical properties of zinc sulfide quantum dots. *Chem Eng J*. 2012;209:113–117.
3. Kimling J, Maier M, Okenve B, Kotaidis V, Ballot H, Plech A. Turkevich method for gold nanoparticle synthesis revisited. *J Phys Chem B*. 2006;110(32):15700–15707.
4. Ghosh D, Sarkar D, Girigoswami A, Chattopadhyay N. A fully standardized method of synthesis of gold nanoparticles of desired dimension in the range 15 nm-60 nm. *J Nanosci Nanotechnol*. 2011;11(2):1141–1146.
5. Frens G. Particle size and sol stability in metal colloids. *Kolloid-Z.u.Z.Polymere*. 1972;250(7):736–741.
6. Dwivedi P, Nayak V, Kowshik M. Role of gold nanoparticles as drug delivery vehicles for chondroitin sulfate in the treatment of osteoarthritis. *Biotechnol Prog*. 2015;31(5):1416–1422.
7. Jung S, Bang M, Kim BS, et al. Intracellular gold nanoparticles increase neuronal excitability and aggravate seizure activity in the mouse brain. *PLoS One*. 2014;9(3):e91360.
8. Abou Neel EA, Bozec L, Perez RA, Kim HW, Knowles JC. Nanotechnology in dentistry: prevention, diagnosis, and therapy. *Int J Nanomedicine*. 2015;10:6371–6394.
9. Nguyen DT, Kim DJ, Kim KS. Controlled synthesis and biomolecular probe application of gold nanoparticles. *Micron*. 2011;42(3):207–227.
10. Fei L, Perrett S. Effect of nanoparticles on protein folding and fibrillogenesis. *Int J Mol Sci*. 2009;10(2):646–655.
11. Liu P, Yang X, Sun S, et al. Enzyme-free colorimetric detection of DNA by using gold nanoparticles and hybridization chain reaction amplification. *Anal Chem*. 2013;85(16):7689–7695.
12. Posch C, Latorre A, Crosby MB, et al. Detection of GNAQ mutations and reduction of cell viability in uveal melanoma cells with functionalized gold nanoparticles. *Biomedical Microdevices*. 2015;17(1):15.
13. Smith MR, Boenzli MG, Hindagolla V, et al. Identification of gold nanoparticle-resistant mutants of *Saccharomyces cerevisiae* suggests a role for respiratory metabolism in mediating toxicity. *Appl Environ Microbiol*. 2013;79(2):728–733.
14. Shevach M, Maoz BM, Feiner R, Shapira A, Dvir T. Nanoengineering gold particle composite fibers for cardiac tissue engineering. *J Mater Chem B*. 2013;1(39):5210–5217.
15. Salata OV. Applications of nanoparticles in biology and medicine. *J Nanobiotechnology*. 2004;2(1):3.
16. Syed MA, Bokhari SH. Gold nanoparticle based microbial detection and identification. *J Biomed Nanotechnol*. 2011;7(2):229–237.
17. Arvizo R, Bhattacharya R, Mukherjee P. Gold nanoparticles: opportunities and challenges in nanomedicine. *Expert Opin Drug Deliv*. 2010;7(6):753–763.
18. Pan Y, Neuss S, Leifert A, et al. Size-dependent cytotoxicity of gold nanoparticles. *Small*. 2007;3(11):1941–1949.
19. El-Brolossy TA, Abdallah T, Mohamed MB, et al. Shape and size dependence of the surface plasmon resonance of gold nanoparticles studied by photoacoustic technique. *Eur Phys J Spec Top*. 2008;153(1):361–364.
20. Zhang XD, Wu D, Shen X, et al. Size-dependent radiosensitization of PEG-coated gold nanoparticles for cancer radiation therapy. *Biomaterials*. 2012;33(27):6408–6419.
21. Wang S-H, Lee C-W, Chiou A, Wei P-K. Size-dependent endocytosis of gold nanoparticles studied by three-dimensional mapping of plasmonic scattering images. *J Nanobiotechnology*. 2010;8(1):33.
22. Tomić S, Đokić J, Vasilijić S, et al. Size-dependent effects of gold nanoparticles uptake on maturation and antitumor functions of human dendritic cells in vitro. *PLoS One*. 2014;9(5):e96584.
23. Condeelis J, Pollard JW. Macrophages: obligate partners for tumor cell migration, invasion, and metastasis. *Cell*. 2006;124(2):263–266.
24. Merzak GJ. Pilkington GJ. Molecular and cellular pathology of intrinsic brain tumours. *Cancer Metastasis Rev*. 1997;16:155–177.
25. Panicker SP, Raychaudhuri B, Sharma P, et al. p300- and Myc-mediated regulation of glioblastoma multiforme cell differentiation. *Oncotarget*. 2010;1(4):289–303.
26. Sontheimer H. Malignant gliomas: perverting glutamate and ion homeostasis for selective advantage. *Trends Neurosci*. 2003;26(10):543–549.
27. Kaushik NK, Kaushik N, Yoo KC, et al. Low doses of PEG-coated gold nanoparticles sensitize solid tumors to cold plasma by blocking the PI3K/AKT-driven signaling axis to suppress cellular transformation by inhibiting growth and EMT. *Biomaterials*. 2016;87:118–130.
28. Kaushik NK, Attri P, Kaushik N, Choi EH. A preliminary study of the effect of DBD plasma and osmolytes on T98G brain cancer and HEK non-malignant cells. *Molecules*. 2013;18(5):4917–4928.
29. Kaushik N, Uddin N, Sim GB, et al. Responses of solid tumor cells in DMEM to reactive oxygen species generated by non-thermal plasma and chemically induced ROS systems. *Sci Rep*. 2015;5(1):8587.
30. Zhou X, Xu W, Liu G, Panda D, Chen P. Size-dependent catalytic activity and dynamics of gold nanoparticles at the single-molecule level. *J Am Chem Soc*. 2010;132(1):138–146.
31. Zhao J. Cancer stem cells and chemoresistance: the smartest survives the raid. *Pharmacol Ther*. 2016;160:145–158.
32. Wang A, Qu L, Wang L. At the crossroads of cancer stem cells and targeted therapy resistance. *Cancer Lett*. 2017;385:87–96.
33. Ahmann FR, Garewal HS, Schifman R, Celniker A, Rodney S. Intracellular adenosine triphosphate as a measure of human tumor cell viability and drug modulated growth. *In vitro Cell Dev Biol*. 1987;23(7):474–480.
34. Berx G, Raspé E, Christofori G, Thiery JP, Sleeman JP. Pre-EMTing metastasis? recapitulation of morphogenetic processes in cancer. *Clin Exp Metastasis*. 2007;24(8):587–597.
35. Al-Hajj M, Wicha MS, Benito-Hernandez A, Morrison SJ, Clarke MF. Prospective identification of tumorigenic breast cancer cells. *Proc Natl Acad Sci U S A*. 2003;100(7):3983–3988.
36. Bao S, Wu Q, McLendon RE, et al. Glioma stem cells promote radioresistance by preferential activation of the DNA damage response. *Nature*. 2006;444(7120):756–760.
37. Doherty M, Smigiel J, Junk D, Jackson M. Cancer stem cell plasticity drives therapeutic resistance. *Cancers (Basel)*. 2016;8(1):E8:8.
38. Ayob AZ, Ramasamy TS. Cancer stem cells as key drivers of tumour progression. *J Biomed Sci*. 2018;25(1):20.
39. Mani SA, Guo W, Liao MJ, et al. The epithelial-mesenchymal transition generates cells with properties of stem cells. *Cell*. 2008;133(4):704–715.
40. Tian X, Liu Z, Niu B, et al. E-cadherin/β-catenin complex and the epithelial barrier. *J Biomed Biotechnol*. 2011;2011(7):1–6.
41. Park J, Ha MK, Yang N, Yoon TH. Flow cytometry-based quantification of cellular Au nanoparticles. *Anal Chem*. 2017;89(4):2449–2456.

Supplementary materials

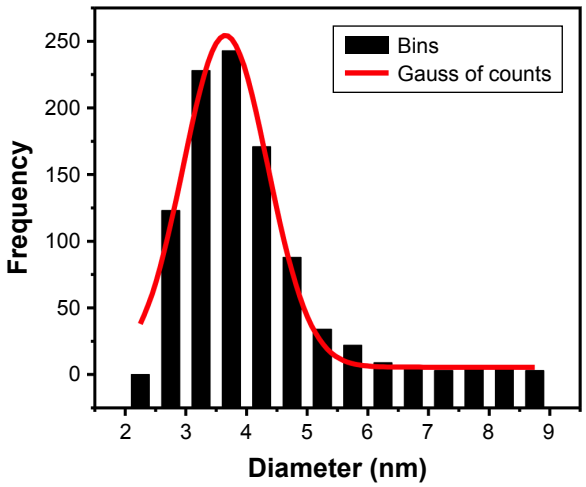

Equation	y=y0 + (A/(w*sqrt(PI/2)))*exp(–2*((x–xc)/w)²)		
Reduced Chi-sqr	227.26907		
Adj. R-square	0.97103		
		Value	**Standard error**
Counts	y0	5.53471	5.64232
Counts	xc	3.65353	0.03803
Counts	w	1.39161	0.08688
Counts	A	434.04716	28.83685
Counts	Sigma	0.69581	
Counts	FWHM	1.6385	
Counts	Height	248.86183	

Figure S1 Size distribution of prepared gold QDs (~4.34 nm [Figure 2A], poly disparity ~19%) with ImageJ software.
Abbreviation: QD, quantum dot.

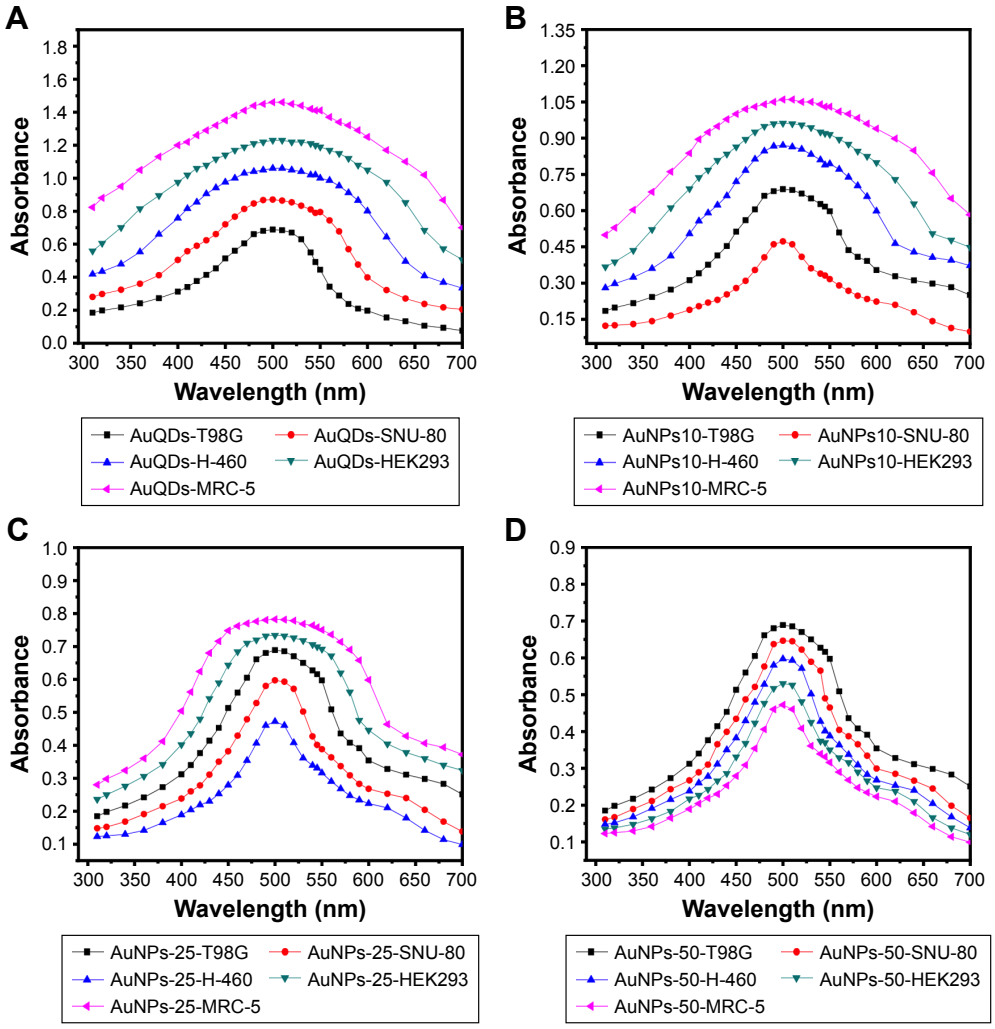

Figure S2 The absorption spectra of MVS-GNPs: quantum dots (<10 nm) (**A**) NPs (10–15 nm) (**B**), NPs (20–30 nm) (**C**), and NPs (45–50 nm) (**D**) with cancer (T98G, SNU-80, H-460) and non-cancerous (HEK293, MRC-5) cells.
Abbreviations: MVS, multivariant-sized; GNP, gold nanoparticle; NP, nanoparticle.

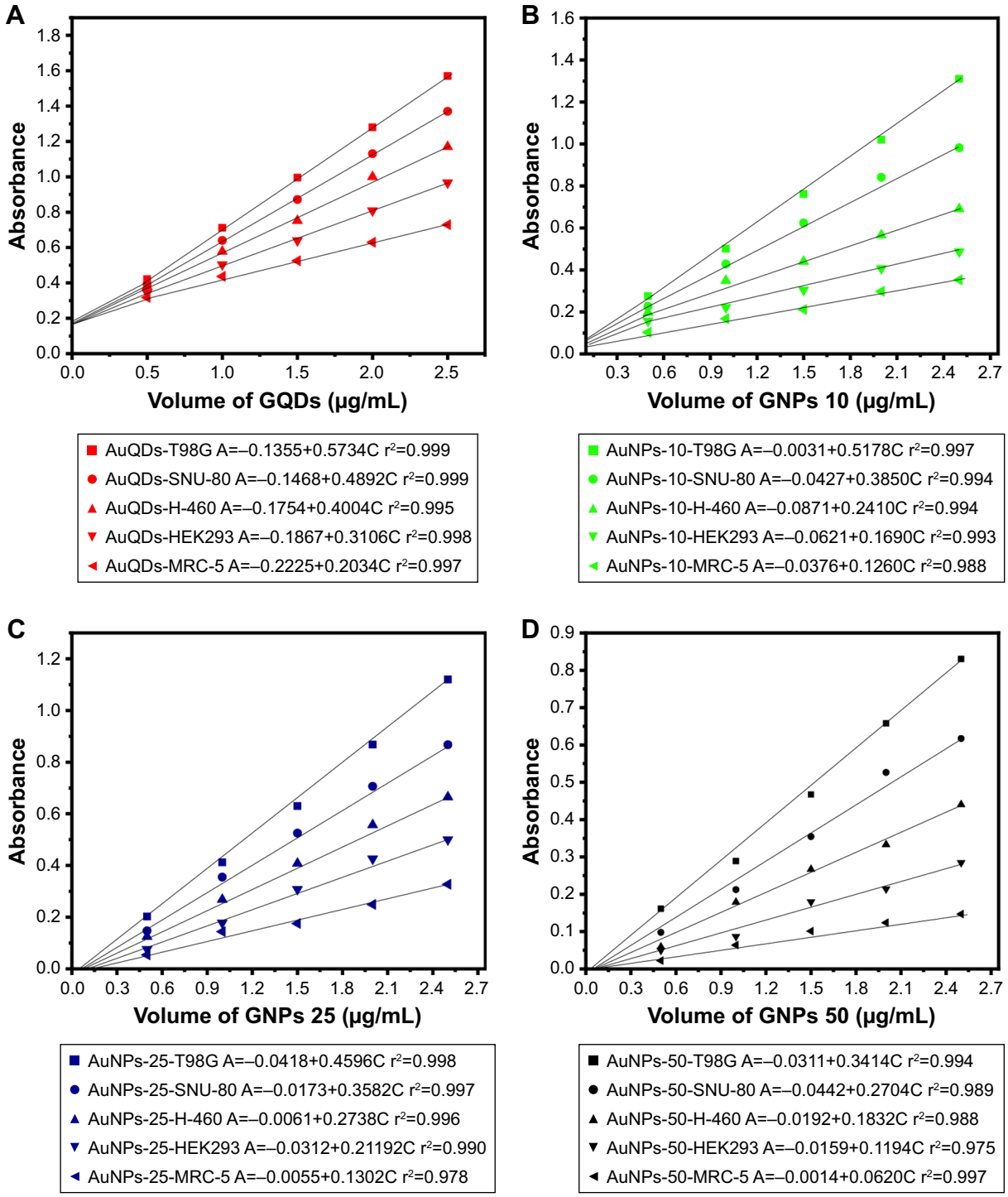

Figure S3 Linear calibration graph of (**A**) GQDs with T98G, SNU-80, H-460, HEK293, and MRC-5 cells, (**B**) GNPs (10–15 nm) with T98G, SNU-80, H-460, HEK293, and MRC-5 cells, (**C**) GNPs (20–30 nm) with T98G, SNU-80, H-460, HEK293, and MRC-5 cells, and (**D**) GNPs (45–50 nm) with T98G, SNU-80, H-460, HEK293, and MRC-5 cells, respectively.

Abbreviations: GQD, gold quantum dot; GNP, gold nanoparticle.

Table S1 Optical parameters of gold quantum dots (GQDs) with different type of cells (GQDs-T98G, GQDs-SNU-80, GQDs-H460, GQDs-HEK293, GQDs-MRC-5)

S.No.	Parameters	GQDs-T98G	GQDs-SNU-80	GQDs-H460	GQDs-HEK293	GQDs-MRC-5
1	Temperature of solutions (°C)	25°C±1°C	25°C±1°C	25°C±1°C	25°C±1°C	25°C±1°C
2	Wavelength (nm)	500	500	500	500	500
3	Spectra range (nm)	300–700	300–700	300–700	300–700	300–700
4	Beer's law limit (µg/mL)	0.5–2.5	0.5–2.5	0.5–2.5	0.5–2.5	0.5–2.5
5	Molar absorptivity (L/mol/cm)	0.628×10^{3}	0.548×10^{3}	0.468×10^{3}	0.386×10^{3}	0.291×10^{3}
6	Linear regression equation	A=–0.1355+0.5734C	A=0.1468+0.4892C	A=–0.1754+0.4004C	A=–0.1867+0.3106C	A=–0.2225+0.2034C
7	$\pm ts_a$	1.215×10^{-3}	3.399×10^{-3}	8.424×10^{-3}	2.792×10^{-3}	1.680×10^{-3}
8	$\pm ts_b$	7.339×10^{-4}	2.049×10^{-3}	5.081×10^{-3}	1.683×10^{-3}	1.012×10^{-3}
9	Correlation coefficient (r^2)	0.999	0.999	0.995	0.998	0.997
10	Variance (So^2 of calibration line)	4.494×10^{-6}	4.830×10^{-5}	4.426×10^{-4}	8.082×10^{-5}	6.822×10^{-5}
11	Detection limit (µg/mL)	0.012	0.046	0.165	0.095	0.134
12	Quantitation limit (µg/mL)	0.036	0.142	0.525	0.289	0.406

Table S2 Optical parameters of gold nanoparticles with different type of cells (GNPs-10-T98G, GNPs-10-SNU-80, GNPs-10-H460, GNPs-10-HEK293, and GNPs-10-MRC-5)

S.No.	Parameters	GNPs-10-T98G	GNPs-10-SNU-80	GNPs-10-H460	GNPs-10-HEK293	GNPs-10-MRC-5
1	Temperature of solutions (°C)	25°C±1°C	25°C±1°C	25°C±1°C	25°C±1°C	25°C±1°C
2	Wavelength (nm)	500	500	500	500	500
3	Spectra range (nm)	300–700	300–700	300–700	300–700	300–700
4	Beer's law limit (µg/mL)	0.5–2.5	0.5–2.5	0.5–2.5	0.5–2.5	0.5–2.5
5	Molar absorptivity (L/mol/cm)	0.524×10^{3}	0.392×10^{3}	0.276×10^{3}	0.194×10^{3}	0.141×10^{3}
6	Linear regression equation	A=–0.0031+0.5178C	A=0.0427+0.3850C	A=–0.0871+0.2410C	A=–0.0621+0.1690C	A=–0.0376+0.1260C
7	$\pm ts_a$	1.082×10^{-2}	8.839×10^{-3}	3.677×10^{-3}	1.933×10^{-3}	1.404×10^{-3}
8	$\pm ts_b$	6.529×10^{-3}	5.332×10^{-3}	2.217×10^{-3}	1.166×10^{-3}	8.479×10^{-4}
9	Correlation coefficient (r^2)	0.997	0.994	0.994	0.993	0.988
10	Variance (So^2 of calibration line)	4.376×10^{-5}	5.271×10^{-4}	2.328×10^{-4}	1.308×10^{-4}	1.243×10^{-4}
11	Detection limit (µg/mL)	0.133	0.196	0.209	0.223	0.292
12	Quantitation limit (µg/mL)	0.404	0.596	0.633	0.676	0.884

Table S3 Optical parameters of gold nanoparticles with different type of cells (GNPs-25-T98G, GNPs-25-SNU-80, GNPs-25-H460, GNPs-25-HEK293, and GNPs-25-MRC-5)

S.No.	Parameters	GNPs-25-T98G	GNPs-25-SNU-80	GNPs-25-H460	GNPs-25-HEK293	GNPs-25-MRC-5
1	Temperature of solutions (°C)	25°C±1°C	25°C±1°C	25°C±1°C	25°C±1°C	25°C±1°C
2	Wavelength (nm)	500	500	500	500	500
3	Spectra range (nm)	300–700	300–700	300–700	300–700	300–700
4	Beer's law limit (μg/mL)	0.5–2.5	0.5–2.5	0.5–2.5	0.5–2.5	0.5–2.5
5	Molar absorptivity (L/mol/cm)	0.448×10^{3}	0.346×10^{3}	0.266×10^{3}	0.200×10^{3}	0.130×10^{3}
6	Linear regression equation	A=–0.0418+0.4596C	A=0.0173+0.3582C	A=–0.0061+0.2738C	A=–0.0312+0.2192C	A=–0.0055+0.1302C
7	$\pm ts_a$	7.440×10^{-3}	5.383×10^{-3}	3.578×10^{-3}	3.868×10^{-3}	2.096×10^{-3}
8	$\pm ts_b$	4.485×10^{-3}	3.245×10^{-3}	2.154×10^{-3}	2.332×10^{-3}	1.264×10^{-3}
9	Correlation coefficient (r^2)	0.998	0.997	0.996	0.990	0.978
10	Variance (So^2 of calibration line)	2.621×10^{-5}	2.259×10^{-4}	1.705×10^{-4}	3.115×10^{-4}	2.592×10^{-4}
11	Detection limit (μg/mL)	0.116	0.138	0.157	0.265	0.408
12	Quantitation limit (μg/mL)	0.352	0.419	0.476	0.805	1.236

Table S4 Optical parameters of gold nanoparticles with different type of cells (GNPs-50-T98G, GNPs-50-SNU-80, GNPs-50-H460, GNPs-50-HEK293, and GNPs-50-MRC-5)

S.No.	Parameters	GNPs-50-T98G	GNPs-50-SNU-80	GNPs-50-H460	GNPs-50-HEK293	GNPs-50-MRC-5
1	Temperature of solutions (°C)	25°C±1°C	25°C±1°C	25°C±1°C	25°C±1°C	25°C±1°C
2	Wavelength (nm)	500	500	500	500	500
3	Spectra range (nm)	300–700	300–700	300–700	300–700	300–700
4	Beer's law limit (μg/mL)	0.5–2.5	0.5–2.5	0.5–2.5	0.5–2.5	0.5–2.5
5	Molar absorptivity (L/mol/cm)	0.332×10^{3}	0.246×10^{3}	0.176×10^{3}	0.114×10^{3}	0.588×10^{3}
6	Linear regression equation	A=–0.0311+0.3414C	A=0.0442+0.2704C	A=–0.0192+0.1832C	A=–0.0159+0.1194C	A=–0.0014+0.0620C
7	$\pm ts_a$	7.176×10^{-3}	6.102×10^{-3}	3.013×10^{-3}	1.882×10^{-3}	5.350×10^{-4}
8	$\pm ts_b$	4.328×10^{-4}	3.680×10^{-3}	1.817×10^{-3}	1.135×10^{-3}	3.230×10^{-4}
9	Correlation coefficient (r^2)	0.994	0.990	0.988	0.975	0.972
10	Variance (So^2 of calibration line)	4.418×10^{-4}	5.094×10^{-4}	2.706×10^{-4}	2.486×10^{-4}	2.447×10^{-5}
11	Detection limit (μg/mL)	0.203	0.275	0.296	0.435	0.459
12	Quantitation limit (μg/mL)	0.605	0.834	0.897	1.320	1.391

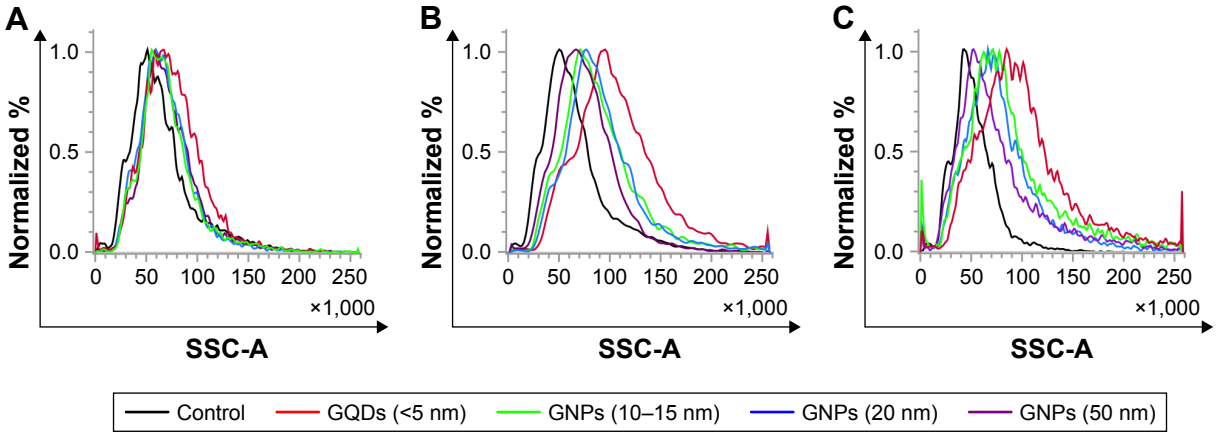

Figure S4 Flow cytometry side scattering intensity (SSC-A) histograms of U87 glioma cells exposed to GQDs (<5 nm), GNPs (10–15 nm), GNPs (20 nm), and GNPs (50 nm) at 100 nM concentrations at 4 hours (**A**), 12 hours (**B**), and 24 hours (**C**) incubation time.
Abbreviations: GQD, gold quantum dot; GNP, gold nanoparticle.